



HAL
open science

Comparative study of ZnO optical dispersion laws

M.-B. Bouzourâa, Y. Battie, S. Dalmaso, M.-A. Zaïbi, M. Oueslati, A. En
Naciri

► **To cite this version:**

M.-B. Bouzourâa, Y. Battie, S. Dalmaso, M.-A. Zaïbi, M. Oueslati, et al.. Comparative study of ZnO optical dispersion laws. Superlattices and Microstructures, 2017, 104, pp.24-36. 10.1016/j.spmi.2017.01.044 . hal-02899477

HAL Id: hal-02899477

<https://hal.univ-lorraine.fr/hal-02899477>

Submitted on 28 Jan 2022

HAL is a multi-disciplinary open access archive for the deposit and dissemination of scientific research documents, whether they are published or not. The documents may come from teaching and research institutions in France or abroad, or from public or private research centers.

L'archive ouverte pluridisciplinaire **HAL**, est destinée au dépôt et à la diffusion de documents scientifiques de niveau recherche, publiés ou non, émanant des établissements d'enseignement et de recherche français ou étrangers, des laboratoires publics ou privés.

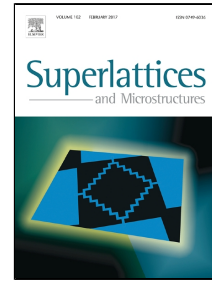


Distributed under a Creative Commons Attribution - NonCommercial - NoDerivatives 4.0
International License

Accepted Manuscript

Comparative study of ZnO optical dispersion laws

M.-B. Bouzourâa, Y. Battie, S. Dalmasso, M.-A. Zaïbi, M. Oueslati, A. En Naciri



PII: S0749-6036(17)30246-X

DOI: 10.1016/j.spmi.2017.01.044

Reference: YSPMI 4808

To appear in: *Superlattices and Microstructures*

Received Date: 30 January 2017

Accepted Date: 31 January 2017

Please cite this article as: M.-B. Bouzourâa, Y. Battie, S. Dalmasso, M.-A. Zaïbi, M. Oueslati, A. En Naciri, Comparative study of ZnO optical dispersion laws, *Superlattices and Microstructures* (2017), doi: 10.1016/j.spmi.2017.01.044

This is a PDF file of an unedited manuscript that has been accepted for publication. As a service to our customers we are providing this early version of the manuscript. The manuscript will undergo copyediting, typesetting, and review of the resulting proof before it is published in its final form. Please note that during the production process errors may be discovered which could affect the content, and all legal disclaimers that apply to the journal pertain.

Highlights

- Ellipsometry is demonstrated as a powerful technique for determining the optical properties of ZnO.
- Tanguy dispersion relationships can be considered as the most appropriate dispersion law for a correct description of ZnO optical properties.
- Tanguy dispersion law takes into account the absorption tail band and the excitonic band of ZnO.
- Temperature-dependent PL measurements are consistent with ellipsometry results using Tanguy dispersion law.

Comparative study of ZnO optical dispersion laws

M.-B. Bouzourâa^{1,2*}, Y. Battie¹, S. Dalmaso¹, M.-A. Zaïbi^{3,4}, M. Oueslati², A. En Naciri^{1*}

¹Université Lorraine, Institut Jean Barriol, LCP-A2MC, Metz, France

²Université de Tunis El Manar, Faculté des Sciences de Tunis, UNP, Tunis, Tunisia

³Université de Tunis, Ecole Nationale Supérieure des Ingénieurs de Tunis, Tunis, Tunisia

⁴Laboratoire de Nanomatériaux et Systèmes des Energies Renouvelables (LANSER) Centre de Recherche de Borj-Cédria Hammam-Lif Tunis, Tunisia

*Corresponding authors: *montassar.bouzouraa@fst.utm.tn, aotmane.en-naciri@univ-lorraine.fr*

ABSTRACT

We report a comparative study between Forouhi-Bloomer, Tauc-Lorentz and Tanguy dispersion laws for determining the reliable dielectric function of crystallized ZnO. ZnO layers were prepared by sol-gel method and deposited on crystalline silicon (c-Si) by spin coating. Spectroscopic ellipsometry (SE) was performed on ZnO/c-Si and each dispersion law was considered in the physical model for fitting SE experimental data. A best agreement was found between measurements and model. This applies in particular to the Tanguy dispersion. The physical parameters such as excitonic energy, optical gap, damping factor, real and imaginary parts of dielectric function were determined and analyzed. The temperature-dependent photoluminescence spectroscopy (PL) measurements were also used to approve the adequate dispersion law for ZnO material. We found by SE and PL measurements that Tanguy law dispersion can be considered as the most appropriate one for a correct description of ZnO optical dielectric function and for the interpretation of the absorption tail band and for the excitonic band of crystallized ZnO. The band-gap energy, excitonic energy and damping factor parameter are determined and analyzed. Their values (3.37 eV, 48 meV and 39 meV, respectively) extracted from ellipsometry are in good agreement with those obtained by PL measurements.

Keywords

Ellipsometry; Optical properties; ZnO; Dispersion law; Photoluminescence.

1. Introduction

Zinc oxide (ZnO) semiconductor has received broad attention due to its versatile properties: wide band gap (~ 3.37 eV at room temperature), large excitonic binding energy (~ 60 meV), good transparency, high electron mobility, size and thermal stability and piezoelectric. These properties make ZnO as a potential and attractive candidate for several applications in: optoelectronics [1, 2], photocatalytic [3], gas sensing [4], UV light emitters [5], solar cells [6] and optical waveguides [7]. Such applications require good knowledge of optical properties of ZnO.

Therefore, it has become essential to control the optical constants of ZnO. Spectroscopic ellipsometry technique is a relevant tool for such optical analysis [8-19]. In the previous works in literature, dispersion laws such as Cauchy [8, 9], Forouhi-Bloomer [8, 9], Tauc-Lorentz [9-12], Tanguy [13, 14] or wavelength-by-wavelength method [20, 21] were used to extract the optical constants of ZnO by modeling spectroscopic ellipsometry (SE) data.

Cauchy's dispersion law is an empirical relationship between the refractive index and wavelength for a particular transparent spectral range. Forouhi-Bloomer relationship obtained from quantum-mechanical theory depicts the optical responses of a variety of amorphous and crystalline semiconductors [8, 9]. Tauc-Lorentz dispersion law combines the empirical Tauc's expression for the band edge onset with the broadening given by the classical Lorentz oscillator. It can be applied for amorphous or crystalline semiconductors.

To our knowledges, no comparison between these models has been found in the literature for the determination of the ZnO dielectric function. In this paper, we give a rigorous analysis of the ellipsometric data using Forouhi-Bloomer, Tauc-Lorentz and Tanguy dispersion laws. SE results are complemented and compared by temperature-dependent photoluminescence (PL) measurements. In particular, the discussion has been performed in order to correlate the band-gap energy and the damping factor with those given by Tanguy dispersion law.

2. Experimental

A large number of elaboration methods have been used for ZnO fabrication such as radio-frequency magnetron sputtering [22], molecular-beam epitaxy [23], pulsed laser deposition [24], metal organic chemical-vapor deposition [25] or sol-gel [26-28]. Among these techniques sol-gel is relatively low cost and enables large-area deposition. In the present work, ZnO thin films were elaborated by sol-gel method.

Zinc acetate dehydrate was dissolved, at ambient temperature, in a mixture solution of 2-methoxyethanol and monoethanolamin. Monoethanolamin is used as a stabilizer and a complexing agent [27]. The concentration of zinc acetate in methoxyethanol was fixed at low value equal to 0.6 mol/L. The molar ratio of Zinc acetate to monoethanolamin was maintained to 1. The mixture was stirred for 2 hours at 60 °C at room temperature. A homogenous and colorless ZnO solution was obtained and was remained stable for several days. The solution obtained was kept 48 hours in aging at room temperature. Then a droplet of particles in suspension was deposited by spin coating at 3000 rpm on silicon substrate. A preheating step at 250°C is used to evaporate the solvents and to remove the organic residuals [20] and an annealing step is necessary to crystallize the ZnO film. This deposition and preheating process was repeated eight times. Finally, the films were annealed at 600 °C in air for 2 hours. This annealing temperature has been chosen in order to obtain a good crystal quality necessary to observe the optical excitonic effect [1]. Experimentally, we have found that repeating of the deposition and preheating process several times leads to the formation of layer with low roughness, a relative homogeneity and the sufficient thickness required for a good sensitivity in ellipsometric measurements. In addition, a number of deposited layers less than five induces the formation of non-continuous film.

The sample morphology was analyzed by scanning electron microscopy (SEM). The measurements were performed on a Zeiss Supra 55VP operating in secondary electron imaging mode with an accelerating voltage of 2 kV and 2.7 mm working distance. The optical response of ZnO layers were investigated by a phase modulated Horiba ellipsometer in the 0.6-4.75 eV spectral range at three incidence angles of 50°, 60° and 70°. The data fit is carried out simultaneously on all incident angles to improve the confidence limit in the data fit. Temperature-dependent PL measurements were carried out, using a monochromator with a 600 grooves/mm grating combined with CCD camera (spectral resolution of 0.23 nm) over a wide range of temperature from 10K to 300K. The excitation wavelength was obtained using the 325 nm (~3.82 eV) line of a 5 mW He-Cd laser.

3. Results and discussion

3.1. Spectroscopy ellipsometric measurements

Ellipsometry measures the changes in the polarization state between incident and reflected light on the samples. The measured values are the ellipsometric angles Ψ and Δ . They are related to

the ratio between the reflection coefficients of the sample for p-polarized light r_p and s-polarized light r_s by [21]:

$$r_p / r_s = \tan \psi e^{i\Delta}, \quad \text{Eq. (A.1)}$$

SE measurements are performed in air at room temperature using a photoelastic modulator ellipsometer. This ellipsometer measures the I_s and I_c parameters related to the ellipsometric angles by [29]:

$$I_s = \sin 2\psi \sin \Delta \quad \text{and} \quad I_c = \sin 2\psi \cos \Delta. \quad \text{Eq. (A.2)}$$

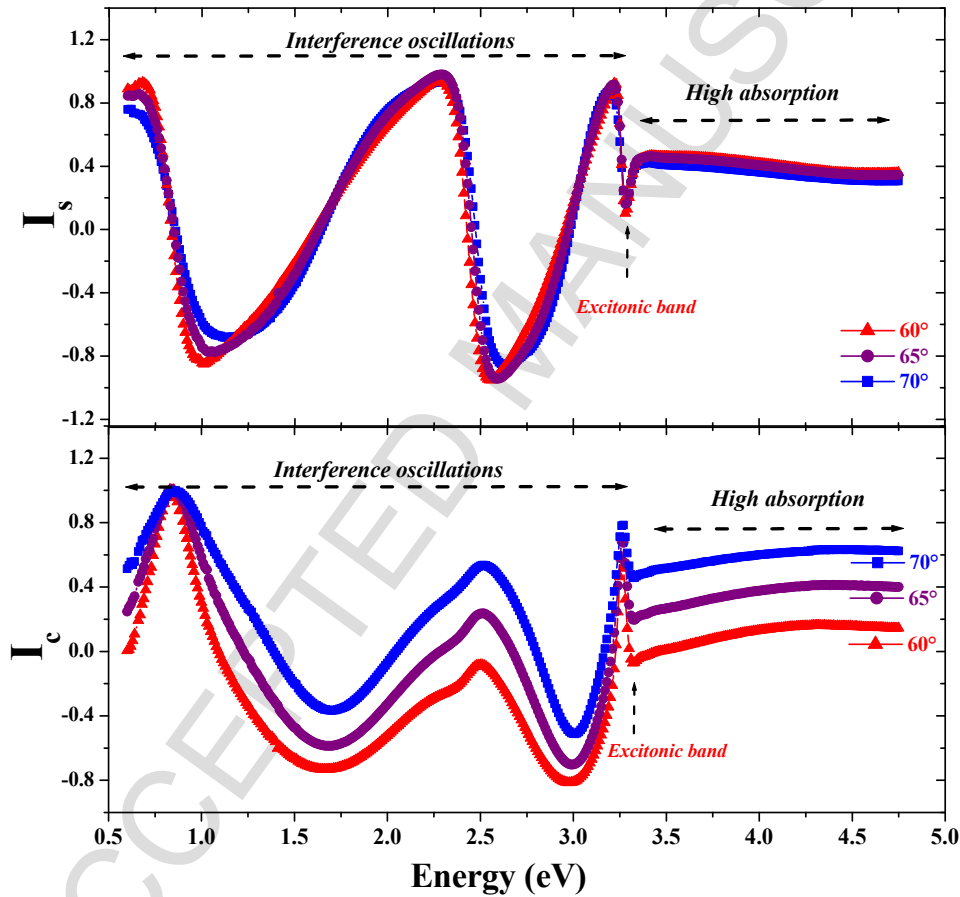


Fig. A.1 Experimental ellipsometric (I_s, I_c) parameters from ZnO/Si measured, at room temperature, in the photon energy range 0.6 to 4.75 eV at incidence angles of 60°, 65° and 70°.

Fig. A.1 shows the variation of I_s and I_c ellipsometric parameters measured from ZnO deposited on crystalline silicon substrate (c-Si). In the spectral range from 0.65 eV to 3.3 eV interferences with large amplitude oscillations can be observed. They are attributed to the multiple internal

reflections and transmissions at the interfaces between the ZnO film and c-Si. In UV range, the absorption phenomenon is taking place resulting from the inter-band transition in ZnO film. This excitonic band, showed in Fig. A.1, traduces the crystalline quality of ZnO layer. The X-Ray diffraction of ZnO has been performed and that give the same results that reported in our previous work where the ZnO is crystallized in a hexagonal wurtzite lattice with c-axis perpendicular to the substrate [30].

For clarity, only the ellipsometry data at incidence angle of 70° is given here, but the same method and results are found for all incidence angles.

A physical model is required to extract optical constants, thickness of different layers and their composition from the analysis of the I_S and I_C ellipsometric parameters. Experimental SE spectra are fitted, by minimizing the following mean-square error using SE data for the three angle incidence simultaneously [31]:

$$\chi^2 = \frac{1}{2N - M - 1} \sum_{i=1}^N \left[\left(I_{C_i(\text{th})} - I_{C_i(\text{exp})} \right) / \delta I_C + \left(I_{S_i(\text{th})} - I_{S_i(\text{exp})} \right) / \delta I_S \right], \text{ Eq. (A.3)}$$

where $I_{C_i(\text{th})}$, $I_{S_i(\text{th})}$ and $I_{C_i(\text{exp})}$, $I_{S_i(\text{exp})}$ are the theoretical and experimental values of I_C and I_S , respectively. N is the number of collected data versus energy, M is the number of unknown parameters of the model, and δI_C and δI_S are the estimated data errors. Generally, the physical model is drawn on sample structure depending on elaboration condition. The surface of elaborated sample and the cross section images have been probed by SEM as can be shown in Fig. A.2. The surface of ZnO/Si is composed of porous layer formed by ZnO granular distributed homogeneously at the surface and separated by voids. The average thickness of ZnO layer is estimated at 235 nm as shown in the cross sectional image. So, the MEB images in Fig A.2 reveals two suppositions: (i) ZnO is an homogeneously layer composed by voids and ZnO like the surface of sample. (ii) ZnO layer is composed by multi-layers, each one is a mixture of ZnO and voids. Hence, two realistic physical models shown in Fig. A.3 are used for SE data analysis. In the modeling, the known parameters are the dielectric functions of c-Si substrate [32] and SiO_2 [33]. Also, the unknown parameters are the thickness of each layer, the volume fractions and dielectric function of ZnO.

The thickness and the composition of each layer in physical model are determined after optimization of the sample structure in the range of ZnO transparency (0.6 eV to 3 eV). Unfortunately, the basic first model composed of one ZnO sublayer (Fig. A.3a) is unsuitable. Indeed large disagreement is observed between experimental and calculated SE parameters I_S

and I_c . A several tests are consisted by layers number, value thickness layers such as they are less than 235 nm and fraction volume of ZnO and voids. As result, we have found that the model shown in Fig. A.3b composed on three ZnO porous sublayers on SiO₂/Si reproduces correctly the experimental spectra. In this model each layer is considered as a mixture between ZnO and voids.

Once the best fit is obtained using Eq. (A.3), numerical results can be determined. The thickness values determined by ellipsometry are $L_1 = 3 \pm 0.1$ nm, $L_2 = 58 \pm 0.3$ nm, $L_3 = 141 \pm 0.2$ nm and $L_4 = 33 \pm 0.2$ nm for, respectively, SiO₂ layer and the three ZnO sublayers. The total thickness value of ZnO obtained by ellipsometry is consistent with that evaluated by SEM (Fig. 2b). The three ZnO sublayers are, in fact, modeled as a mixture of ZnO and voids according to Bruggeman effective medium theory [34]. Table A.1 summarized the composition of each sublayer. The origin of the voids in our film can be attributed to the growth mechanism for ZnO/Si. For example, Gilliot *et al.* [19] have deposited ZnO films synthesized by sol-gel on 50 nm SiO₂ hydrophilic layer on c-Si involving no voids in ZnO layer. As consequence, they are proposed a physical model composed by ZnO sublayer and roughness top sublayer. In our case, the ZnO layers were deposited on 3 nm SiO₂ layer on c-Si inducing a weak density of granular ZnO layer (L_2). This can explain the large volume fraction of voids (37 ± 0.03 %). A condensed ZnO layer (L_3) was obtained after repeating spin-coating deposition eight times. In this layer the voids is reduced to 6%. The top layer (L_4) is considered as roughness layer.

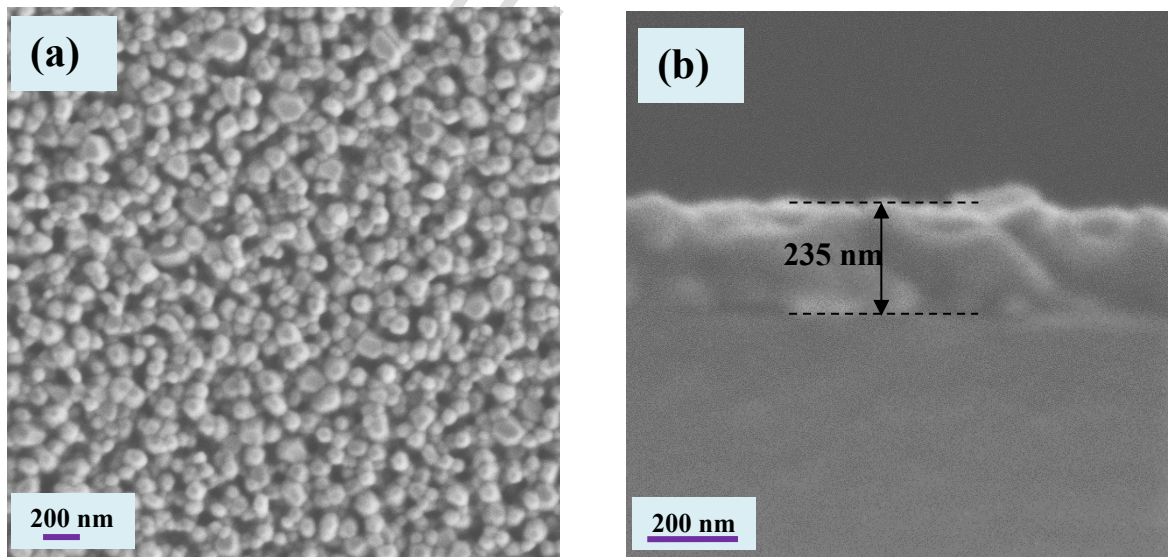


Fig. A.2. SEM images of (a) the surface and the (b) cross section of ZnO/Si sample.

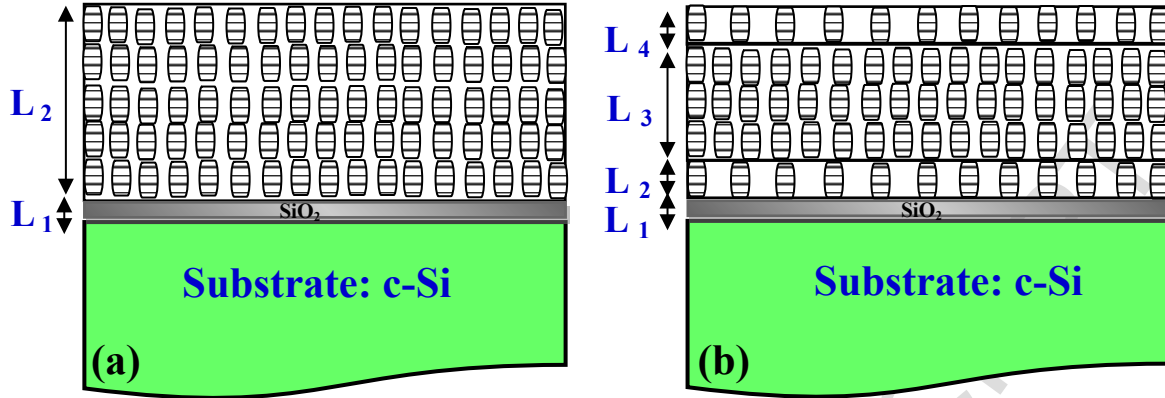


Fig. A.3 Physical model which represents the ZnO/Si sample as (a) two sublayers and (b) four sublayers of ZnO/Si sample.

Table A.1: Composition of each sublayer associated to the model in Fig A.3b.

Sublayer	L ₂	L ₃	L ₄
ZnO	63 ± 0.03 %	94 ± 0.03 %	64 ± 0.03 %
Voids	37 ± 0.03 %	6 ± 0.03 %	36 ± 0.03 %

In addition of structural characterization of sample by ellipsometry, the optical properties of ZnO in each layer were determined by analyzing SE data in the range of 0.6 eV to 4.75 eV. The dielectric function of ZnO were modeled by Tauc-Lorentz (TL), Forouhi-Bloomer (FB) and Tanguy dispersion relationships.

- **Tauc-Lorentz dispersion law:**

In TL model, the imaginary part of the dielectric function combines the empirical Tauc's expression for the band edge onset with the broadening given by the classical Lorentz oscillator [15]:

$$\epsilon_{i, TL}(E) = \frac{1}{E} \times \frac{A_1 \cdot E_0 \cdot C_1 (E - E_g)^2}{(E^2 - E_0^2)^2 + C_1^2 \cdot E^2} \times H(E - E_g). \quad \text{Eq. (A.4)}$$

A_1 is the oscillator strength. E_0 is the energy of the absorption band. C_1 is the broadening parameter associated to the absorption band. E_g is the bandgap energy. $H(E - E_g)$ is the Heaviside function. The real part of the dielectric function is obtained from the Kramers-Kronig

relation [35]:

$$\varepsilon_{r, TL}(E) = \varepsilon_{\infty} + \frac{2}{\pi} \cdot \text{P} \int_E^{\infty} \frac{\xi \cdot \varepsilon_i(\xi)}{g\xi^2 - E^2} d\xi, \quad \text{Eq. (A.5)}$$

ε_{∞} is the dielectric constant at high photon energy. In this TL model, five free parameters (A_1 , E_0 , C_1 , E_g , ε_{∞}) are fitted to determine the dielectric function of ZnO.

- **Forouhi-Bloomer dispersion law:**

Five parameters (A_2 , B , C_2 , E_g and ε_{∞}) are also necessary to fit the FB model [36]. This model that takes into account the number and lifetime of inter-band transitions is based on extinction coefficient and refractive index relationships given by:

$$k_{FB}(E) = \frac{A_2 \cdot (E - E_g)^2}{E^2 - B \cdot E + C_2} \times H(E - E_g), \quad \text{Eq. (A.6)}$$

$$n(E) = \sqrt{\varepsilon_{\infty}} + \frac{1}{\pi} \cdot \text{P} \int_{-\infty}^{\infty} \frac{k(E') - k(\infty)}{E' - E} dE', \quad \text{Eq. (A.7)}$$

where, A_2 represents the oscillator strength, $B/2$ and C_2 are assimilated to the absorption band energy and width, respectively, E_g and ε_{∞} have the same meanings as defined for TL model.

- **Tanguy dispersion law:**

The Tanguy dispersion relationships which take into account the electronics transitions around the band gap and the Wannier excitonic effect on semi-conductor's complex dielectric function are given by [37]:

$$\varepsilon(E) = \varepsilon_{\infty} + \frac{a}{b - (E + i\Gamma)^2} + A_3 (\tilde{\varepsilon}_u(E) + \tilde{\varepsilon}_b(E)), \quad \text{Eq. (A.8)}$$

with

$$\tilde{\varepsilon}_u(E) = \frac{2\sqrt{R}}{(E + i\Gamma)^2} \left[-2g_u \left(\sqrt{\frac{R}{E_g}} \right) + g_u \left(\sqrt{\frac{R}{E_g - E - i\Gamma}} \right) + g_u \sqrt{\frac{R}{E_g + E + i\Gamma}} \right], \quad \text{Eq. (A.9)}$$

$$\tilde{\varepsilon}_b(E) = \frac{2\sqrt{R}}{(E + i\Gamma)^2} \left[-2g_b \left(\sqrt{\frac{R}{E_g}} \right) + g_b \left(\sqrt{\frac{R}{E_g - E - i\Gamma}} \right) + g_b \left(\sqrt{\frac{R}{E_g + E + i\Gamma}} \right) \right], \quad \text{Eq. (A.10)}$$

A_3 is an amplitude factor, R is the energy of the fundamental excitonic state, Γ is the damping factor, a and b are the Sellmeier coefficients and g_u and g_b are functions, respectively, expressing the contributions of bound and unbound excitons defined as:

$$g_u(z) = \ln(z) + \psi(z) + \frac{1}{2z}, \quad \text{Eq. (A.11)}$$

$$g_b(z) = -2\psi(z) - \pi \cot \pi z - \frac{1}{z}, \quad \text{Eq. (A.12)}$$

where ψ is the digamma function and \cot is the cotangent function.

The comparison between measurement and calculated ellipsometric parameters is shown in Fig. A.4. The best fitting is obtained for the Tanguy dispersion law. Comparing to FB and TL dispersion laws, we can see in the insert of Fig. A.4 (spectral range from 3.20 to 4.75 eV) that the good agreement between measurement and calculated I_c and I_s is obtained by the Tanguy relationships. In the spectral range (0.65 to 3.20 eV), the three dispersions laws reproduce correctly the SE data confirming the validity of the selected physical model given in Fig. A.3b. However, the Tanguy law is the only one that reproduces the experimental data in large spectral range (0.65 to 4.75 eV).

The fitted parameters for the Tanguy, FB and TL dispersion laws and the mean-square error χ^2 values are summarized in Table A.2. The smallest of all is given for Tanguy model. ϵ_∞ values are large than 1 as it is well known for semiconductor material. Generally the value of ϵ_∞ reported in literature is ranging from 1.54 to 2.66 [19, 38-40]. This is the case for the Tanguy dispersion law comparing to higher values obtained by FB and TL.

Concerning the amplitude factor A (A_1, A_2, A_3), the comparison between these dispersion laws is not effective because the relationships are different. It is well known that A factor drastically affects the amplitude of optical transition near the band gap as can be seen in Fig. A.5. As reported in literature, the A value depend on ZnO structure and the layer density according to the elaboration methods [19, 38, 40]. In our case, the A_1 value is less than the one obtained for ZnO grown by epitaxy [41]. This can be explained by the presence of residual defects in the zinc oxide granular. This remark is also valid for A obtained by FB and TL models by comparing the values to those given in Refs. [9, 18] for FB and in Ref. [10] for TL.

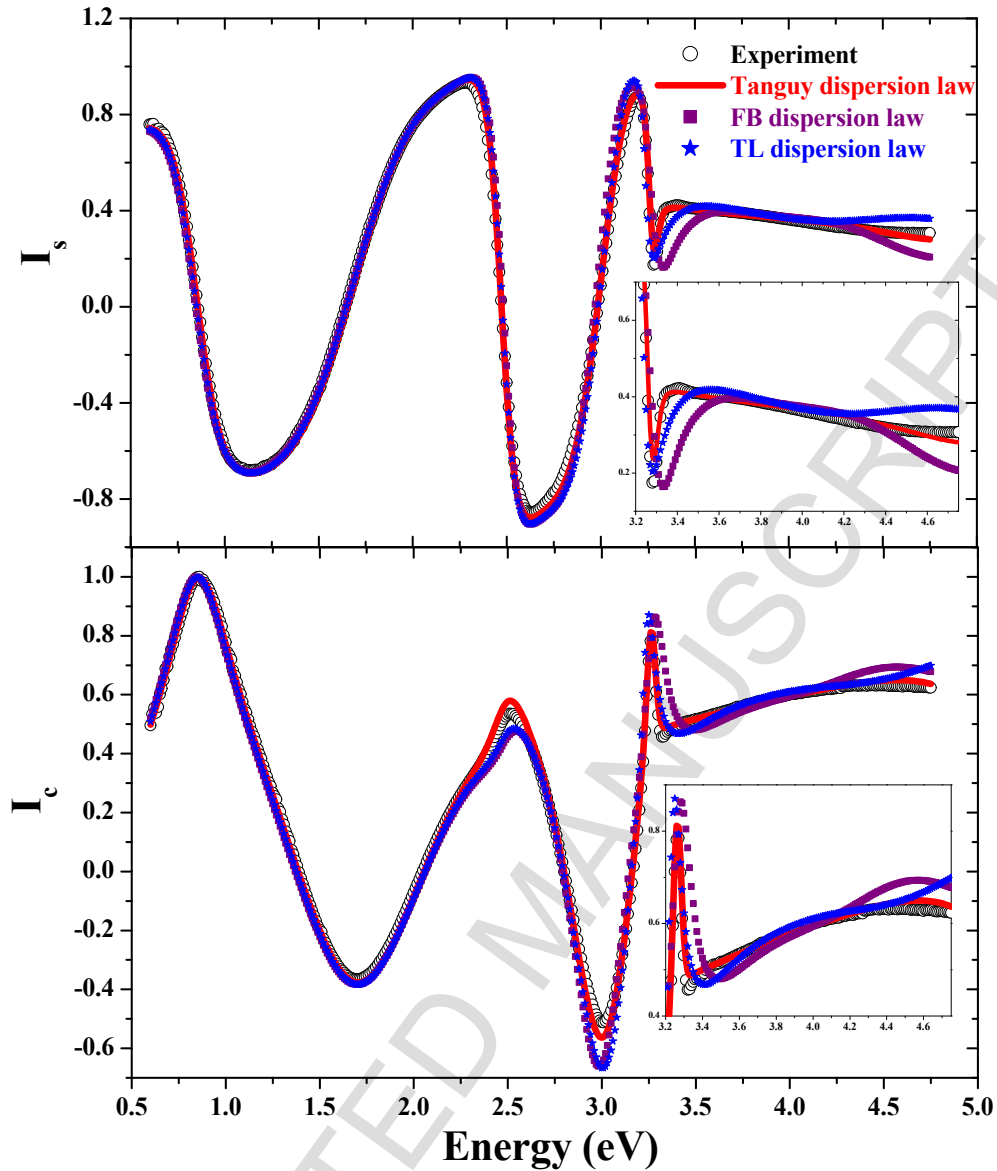


Fig. A.4 Comparison between calculated and measured ellipsometric parameters from ZnO/Si sample.

The optical gap E_g (3.37 eV) value determined by Tanguy relationships, given in Table A.2, is in agreement with those reported in literature [13, 38, 39, 41, 42]. However the exciton energy R value (48 meV) determined by Tanguy dispersion law is found to be less than the known value (60 meV) of perfect crystallized ZnO. It turns out that the R values change with the crystal quality of ZnO and elaboration methods. The reported values in literature are ranging from 45 meV to 78 meV [13, 38, 39, 41, 42]. Here, the ZnO layer should fail due to defects in granular material. As consequence the exciton energy value is affected.

The $B/2$ and E_0 values obtained by FB and TL corresponding to excitonic absorption band energy are blue shifted comparing to one given by Tanguy as can be shown in Fig. A.5. This

result can be explained by the incorrectly fitting of excitonic band by FB and TL (see the insert in Fig. A.4).

Concerning the Γ damping factor, the obtained value (39 meV) is consistent with the ZnO sol-gel quality. Indeed Γ value decreases with crystal quality [19, 30, 38]. The C (C_1 , C_2) values of broadening parameter associated to the absorption peak parameter are also given in Table A.2. C is large for ZnO amorphous. In our case the values obtained by FB and TL reflect the crystalline structure of ZnO layers [9, 18].

Table A.2: Tanguy, FB and TL ZnO parameters. For comparison, χ^2 values are also given.

Tanguy	χ^2	ϵ_∞	A_1 (eV ^{3/2})	E_g (eV)	R (meV)	Γ (meV)
dispersion law	4	2.37 ± 0.03	19.39 ± 0.6	3.37 ± 0.01	48 ± 2	39 ± 1
FB	χ^2	ϵ_∞	A_2 (\emptyset)	E_g (eV)	B (eV)	C_1 (eV ²)
dispersion law	22	3.72 ± 0.02	0.2 ± 0.008	3 ± 0.01	6.82 ± 0.02	11.72 ± 1
TL	χ^2	ϵ_∞	A_3 (eV)	E_g (eV)	E_0 (eV)	C_2 (eV)
dispersion law	26	3.05 ± 0.01	203.5 ± 6	3.12 ± 0.01	3.30 ± 0.01	0.37 ± 0.01

Using the fitting parameters in Table A.2, the calculated imaginary and real parts of dielectric function of ZnO are given in Fig. A.5. From 0.65 to 3.25 eV, the imaginary part of dielectric functions by Tanguy shows an absorption tail in visible unlike TL and FB (see the insert in Fig. A.5). This indicating the occurrence of the defects in the film as can be expected for ZnO elaborated by sol-gel technical. The excitonic band centered at around ~ 3.4 eV is observed for the Tanguy. According to the results in Table A.2 and Fig. A.5, the excitonic band for FB and TL are blue shifted, more broadened and more intense than the ones obtained from Tanguy. Beyond 3.4 eV, only the Tanguy dispersion law present a typical absorption almost constant [1]. Therefore, we consider the Tanguy dispersion formula as the most appropriate dispersion law to the absorption tail band and the typical excitonic band crystallized ZnO.

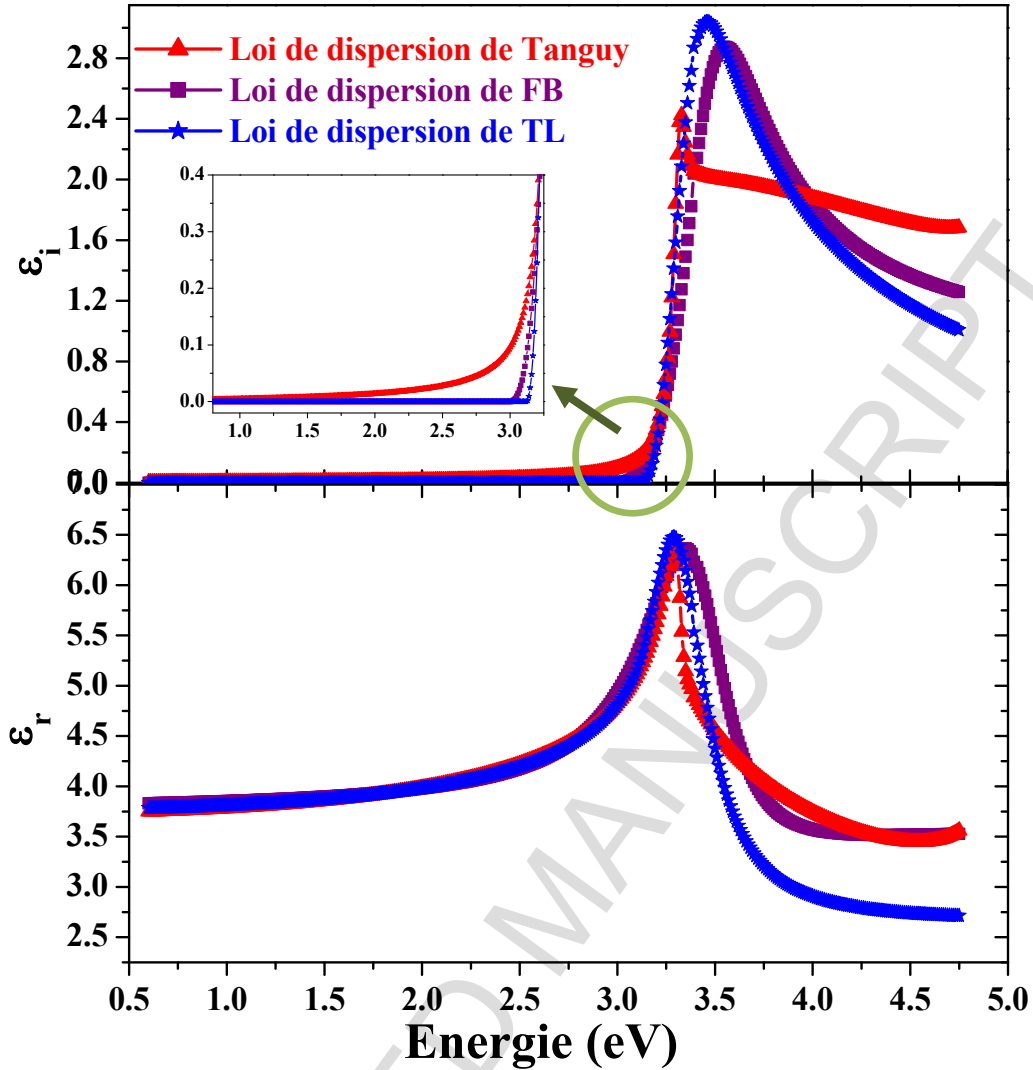


Fig. A.5 Imaginary and real parts of dielectric function of ZnO determined by Tanguy, FB, TL.

3.2. Temperature-dependent PL

Temperature dependent photoluminescence measurements were performed in order to extract the excitonic energy, the band gap energy and the damping factor of ZnO and to correlate them with SE results.

Fig. B.1 shows the temperature dependence on PL spectra of ZnO/Si from 10 K to 300 K. At 10 K, three emissions near ZnO band edge at 3.373, 3.326 and at 3.242 eV were clearly resolved and attributed to the emission of free exciton (FX) [1, 43, 44], donor-bound exciton (AX) [43] and donor-acceptor pairs (DAP) [43], respectively. The other bands located at around 3.168, 3.098 and 3.000 eV are may be assimilated to the first order longitudinal optical (1LO) phonon replica of DAP (DAP-1LO) and (DAP-2LO), respectively.

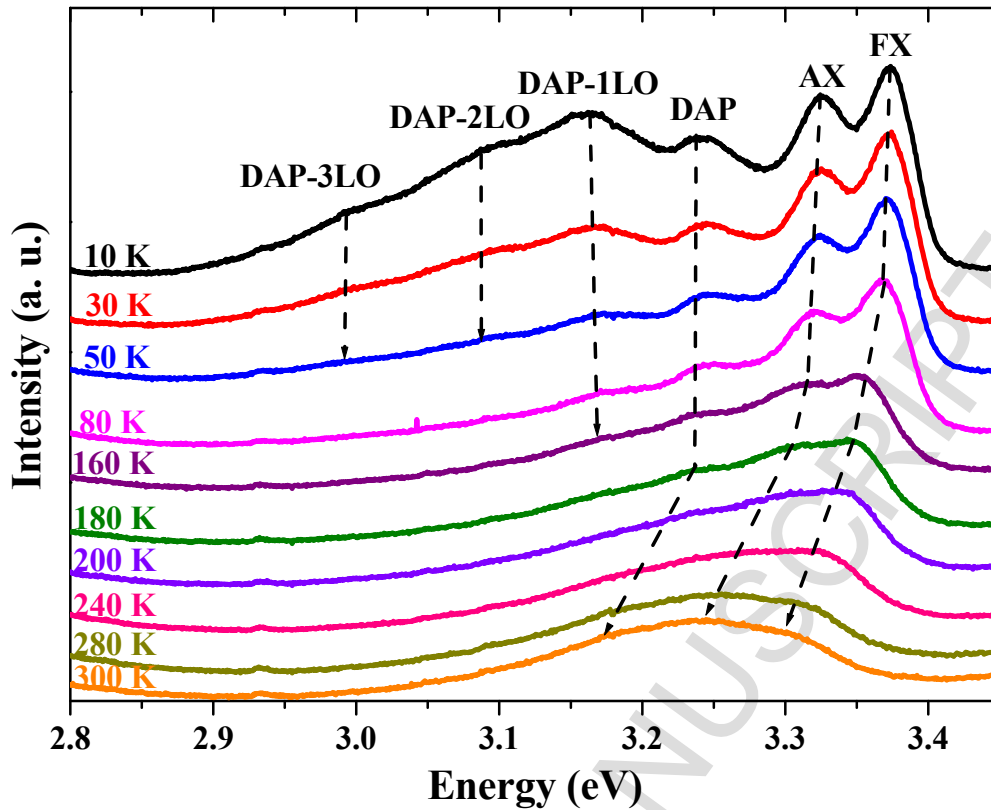


Fig. B.1 Temperature-dependent PL spectra of near-band-edge emissions of ZnO/Si.

It should be noted that the energy difference between the zero phonon line and 1LO phonon replica line (78 meV) is somewhat larger than the energy of a LO phonon (72 meV) calculated by Klingshirn [45]. Nevertheless, Jiang *et al.* [43] reported 66 meV for ZnO elaborated by atmospheric pressure metal–organic chemical vapor deposition on Al_2O_3 substrate. In addition, this result has been observed in ZnO crystal whose absorption spectra have shown a $\sim 10\%$ (error fraction) softening of 1LO phonon energy compared to ZnO crystals [46]. Toyozawa *et al.* [47] have explained this effect by the exciton–polaron model. By taking into account this error, our results are in good agreement with literature. Heating the sample from 10 K up to 300 K, we observed the red shift of the transitions with thermal quenching of some bands and disappearance of their transitions. Note that signal was still present at room temperature. In order to understand the different processes, we analyzed the evolution of the integrated intensities, energies and the full width at half maximum (FWHM) as the function of the temperature for the different transitions.

Fig. B.2 presents the decomposition of PL spectra intensity, obtained at 10 K, 80 K, 200 K and 300 K, into Lorentzian multi-bands. Then, the integrated PL intensity corresponding to FX band can be determined for each temperatures.

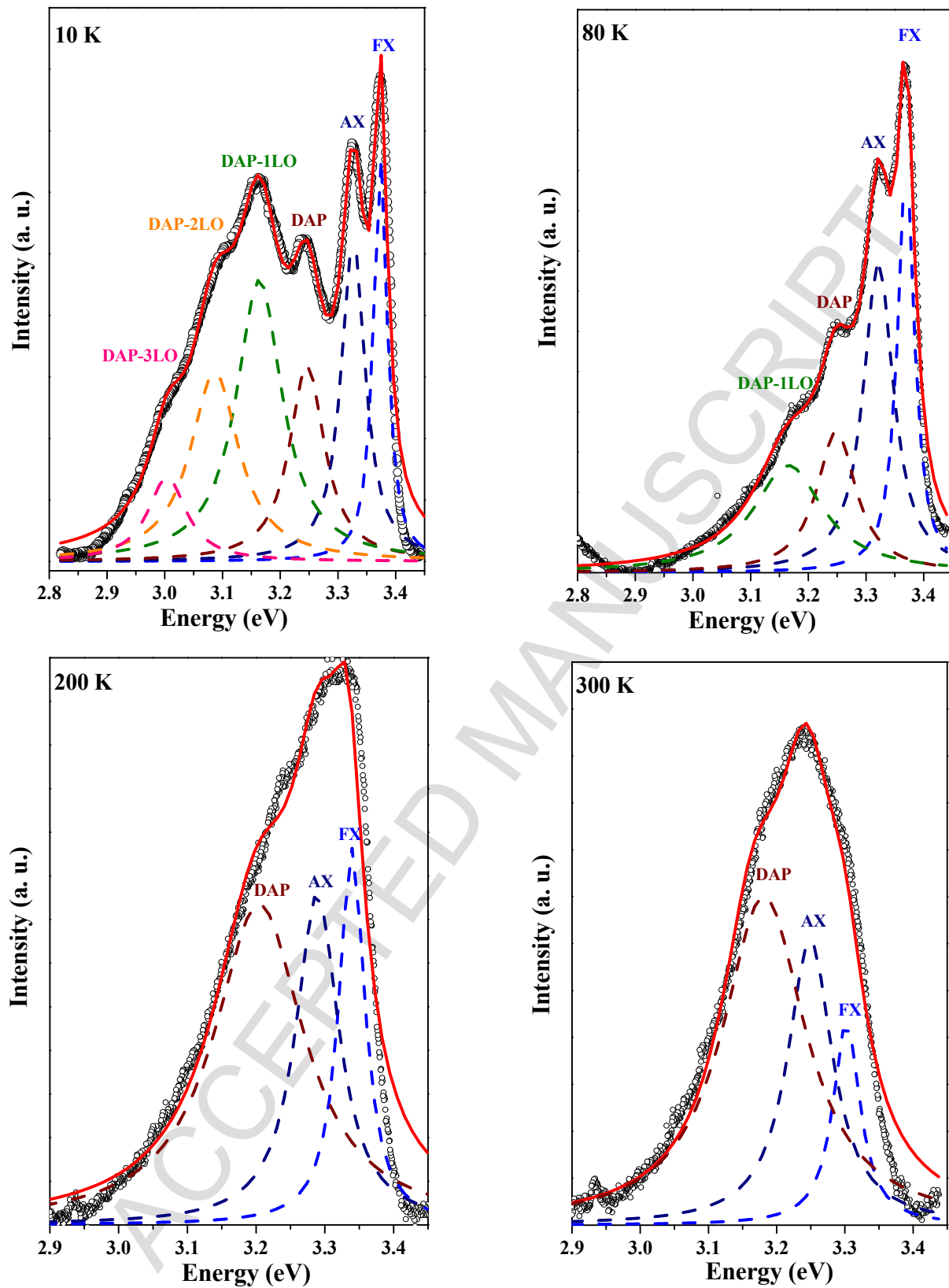


Fig. B.2 The fits of PL spectra into Lorentzian line shape at 10 K, 80 K, 200 K and 300 K.

Fig. B.3 exhibits the temperature (T) dependence of integrated PL intensities (I) for FX band. We can clearly see that at high temperature, the emission intensity decreases with temperature due to the thermal quenching.

The temperature-dependent quenching of FX intensity can be fitted by a typical Arrhenius formula:

$$I = I_0 / \left(1 + A \exp \left(- \frac{E_a}{k_B T} \right) \right), \quad \text{Eq. (B.1)}$$

where I_0 is the peak intensity at $T=0$ K, A is a constant, E_a (eV) is the activation energy of the thermal quenching process, and k_B is the Boltzmann constant.

From the fit, E_a was estimated to be 46 ± 1 meV. The FX thermal activation energy for the ZnO represents the excitonic energy [48]. This value is well consistent with binding energy calculated by Tanguy as seen in Table A.2.

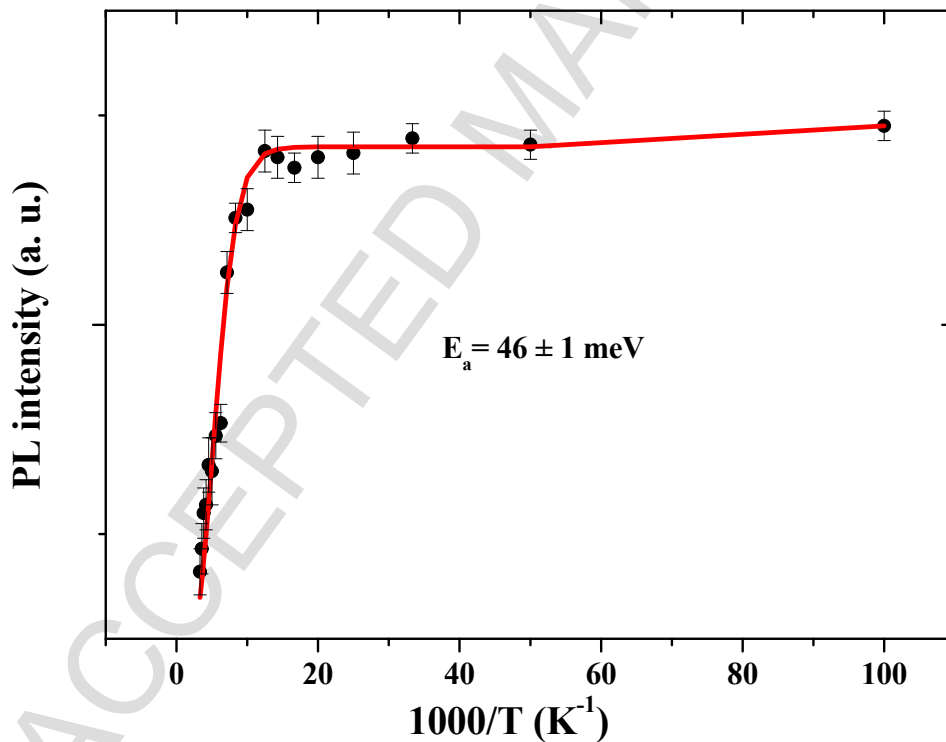


Fig. B.3 Integrated PL intensity of FX band dependence on temperature. Solid line is the fitting of the experimental data using Eq. (B.1).

Wang *et al.* [49] have been shown that FX transition energy E_{FX} evolved with temperature similarly that the band gap energy E_g . Thus, both Varshni's and Cody's formula [48, 50] are

valid for E_g and E_{FX} . Temperature dependence of the FX transition energy E_{FX} , reported in Fig. B.4, is fitted using both Varshni's formula [50] and Cody's formula [51].

The Varshni's formula is defined by the equation below:

$$E_{FX}(T) = E_{FX}(0) - (\alpha T^2)/(\beta + T), \quad \text{Eq. (B.2)}$$

where $E_{FX}(T)$ is the temperature-dependent of the FX transition energy, $E_{FX}(0)$ is the FX energy at $T=0$, α and β are constants specific to ZnO such as β is the Debye temperature. As shown in top of Fig. B.4, the values of Varshni parameters $E_{FX}(0)$, α and β are equal to 3.37 eV, 2.5 ± 0.04 meV/K and 2700 ± 50 K, respectively. These values are in agreement with that reported by Nam *et al.* [44]. However, β value is higher than the Debye temperature (900 K) [52]. The FX temperature-dependence is, also, fitted using Cody approach giving by Cody's approach:

$$E_{FX}(T) = E_{FX}(0) - k/\left(\exp\left(\frac{\theta}{T}\right) - 1\right), \quad \text{Eq. (B.3)}$$

where $E_{FX}(T)$ and $E_{FX}(0)$ have the same meanings as defined for Varshni formula, k is a constant and θ is related to the average phonon frequency and generally taken to represent the Einstein temperature. The Cody parameters obtained from fitting, in bottom of Fig. B.4, are $E_{FX}(0) = 3.37$ eV, $k = 0.12 \pm 0.02$ eV and $\theta = 300 \pm 30$ K. We note that the temperature given by Cody is close to the Einstein temperature (250 K) for ZnO [49]. We note that Cody's formula yields a good fit and parameter acceptable physical result.

The ZnO band-gap energy (E_g) value at room temperature can be calculated using Eq. (B.3) and adding the excitonic energy E_a that was found to be 46 meV (Fig B.4) [53]:

$$E_g = E_n + E_a/n^2, \quad \text{Eq. (B.4)}$$

where E_n is the transition energy for free exciton corresponding to one among the three valence bands (A, B or C) and n is the main quantum number. In our case, n equal to 1 and E_n is the free exciton energy for A valence band (E_{FX})[1]. The ZnO band-gap energy at room temperature is estimated to ~ 3.35 eV using Eq. (B.4). The value is very close to that calculated by Tanguy dispersion law (3.37 eV).

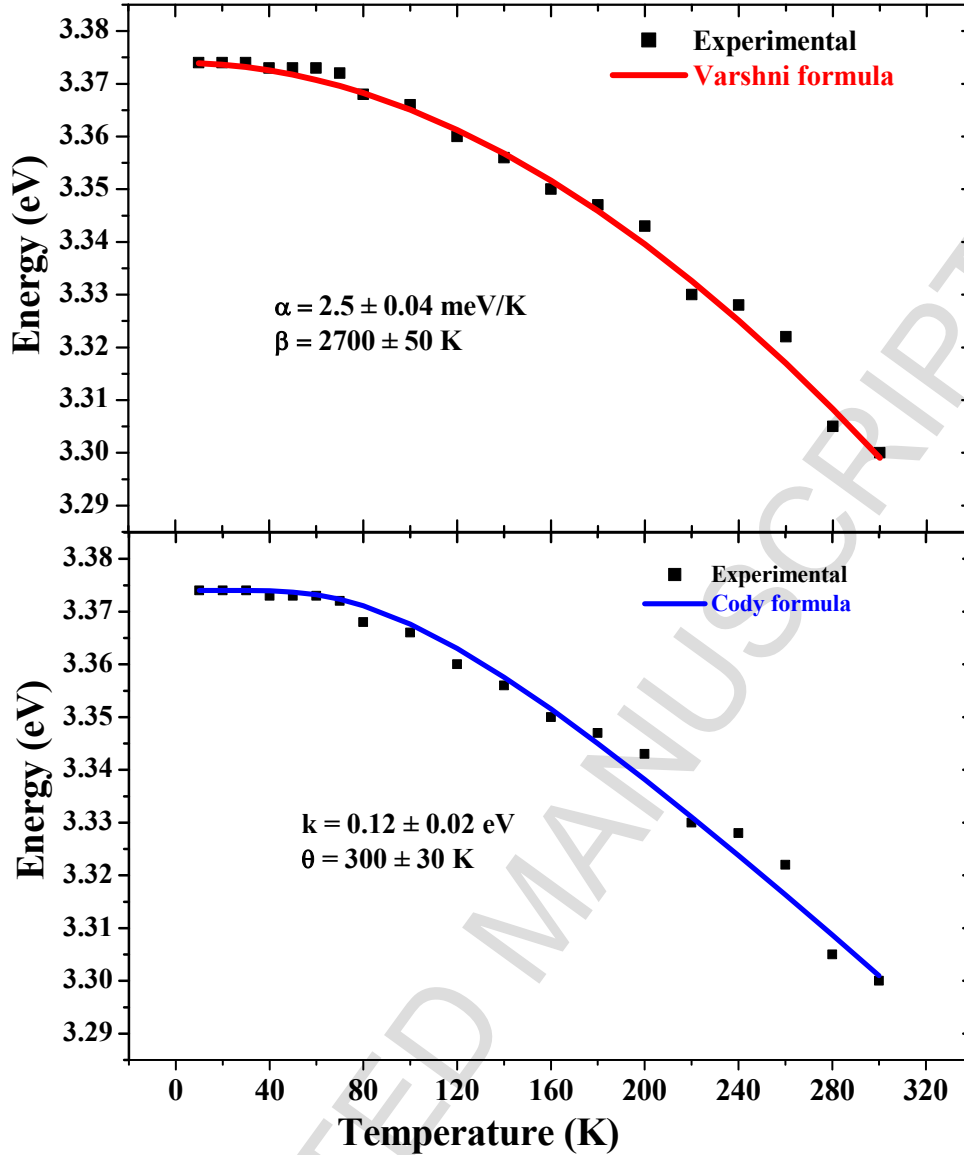


Fig. B.4 Temperature dependence for FX transition fitted by Varshni formula on the top and by Cody formula on the bottom.

The dependence FWHM of FX as function of the temperature is presented in Fig B.5. The experimental data for Γ could be simulated by the following theoretical formula [51, 54]:

$$\Gamma(T) = \Gamma_0 + \gamma_{ph}T + \Gamma_{LO}/\exp\left(\frac{\hbar\omega_{LO}}{k_B T - 1}\right), \quad \text{Eq. (B.5)}$$

where Γ_0 is the background impurity broadening (i.e., inhomogeneous broadening) due to temperature-independent mechanisms, such as impurity, dislocation, and surface scattering, γ_{ph} is the coupling strength of an exciton-acoustic phonon interaction, Γ_{LO} is the strength of the exciton-LO-phonon coupling and $\hbar\omega_{LO}$ is the LO-phonon energy.

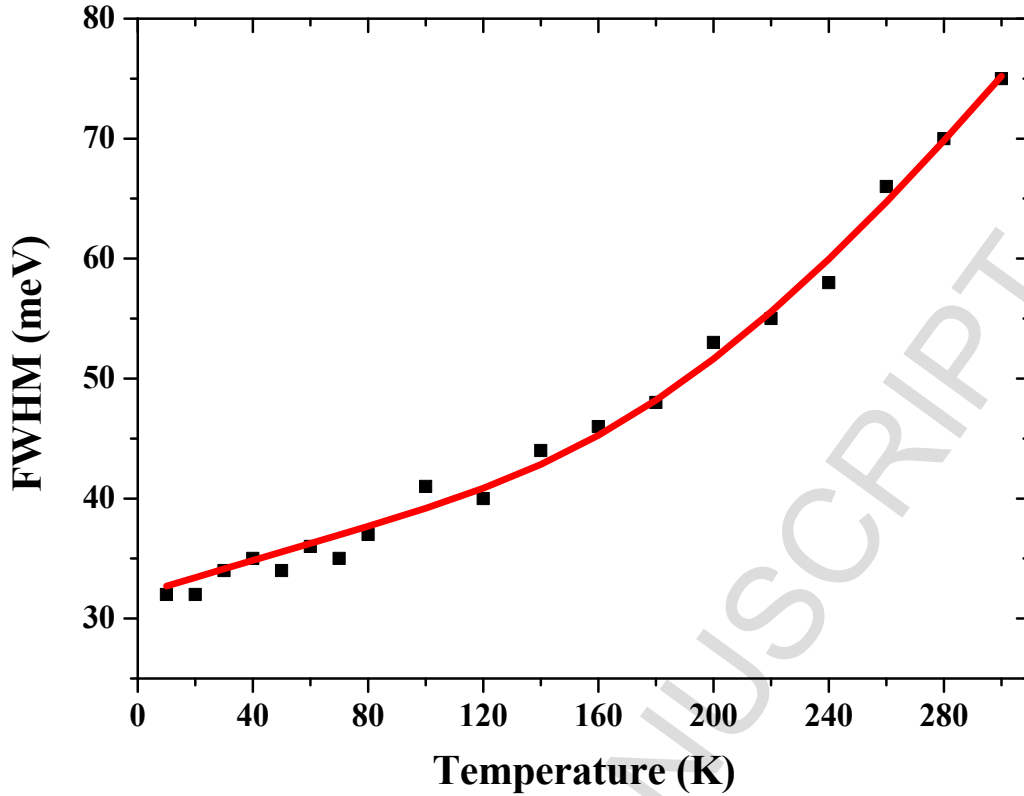


Fig. B.5 FWHM of FX peak versus temperature. Solid line is the fitting experimental result using Eq. (B.4).

Straight line represents the best fit obtained using Eq (B.5) with the following parameters $\Gamma_0=31 \pm 0.5$ meV, $\Gamma_{LO}= 150 \pm 10$ meV and $\gamma_{ph} = 0.07 \pm 0.005$ meV/K. These results are in overall in good agreement with those obtained by Nam *et al.*[44]. Nevertheless, slightly higher value of Γ_{LO} may be correlated with the predominance of the first replica phonon at low temperature as show in Fig. B.1. Moreover, Γ_0 (31 meV) reveals the presence of defects in ZnO layers and its value remained slightly lower than Γ (39 meV) obtained by Tanguy dispersion law.

4. Conclusions

In summary, Tanguy dispersion relation was demonstrated to be as the most appropriate dispersion law for a correct description of ZnO optical properties. In the present work, a comparative study of the results obtained by three dispersion laws, namely, Forouhi-Bloomer, Tauc-Lorentz and Tanguy is given and analyzed.

ZnO synthesized by sol-gel and deposited by spin coating on crystalline silicon (ZnO/Si). The ZnO/Si sample was characterized by SEM, ellipsometry and temperature dependent PL over a

wide range of 10 K-300 K. The physical model for analyzing spectroscopic ellipsometry data was based on the observation of surface and cross sectional SEM images. We found that the consideration of the porosity of ZnO layer in the physical model greatly enhances the fit quality. The Tanguy dispersion law describes correctly the optical properties of ZnO over the spectral range 0.6 to 4.75 eV. In addition of dielectric function of ZnO, Tanguy relationships allow determining other physical parameters such as the optical gap (3.37 eV), excitonic energy (48 meV) and the damping factor (39 meV). Temperature-dependent PL measurements confirm this statement of ellipsometry results about the Tanguy dispersion law.

Acknowledgment

The authors would like to acknowledge Jean-Luc Pierrot and Pascal Franchetti (LCP-A2MC) for SEM images and technical assistance in PL measurements.

References

- [1] Ü. Özgür, Y. I. Alivov, C. Liu, A. Teke, M. A. Reshchikov, S. Doğan, V. Avrutin, S.J. Cho, H. Morkoç, *J. Appl. Phys.* 98 (2005) 041301.
- [2] S. Sharma, S. Vyas, C. Periasamy, P. Chakrabarti, *Superlattices and Microstructures* 75 (2014) 378-389.
- [3] K. N. Abbas, N. Bidin, *Applied Surface Science* 394 (2017) 498–508.
- [4] R. Joaniso, O.K. Tan, *Semiconductor Gas Sensors*, Woodhead Publishing, Cambridge, 2013.
- [5] M. Norek, G. Łuka, M. Włodarski, *Applied Surface Science* 384 (2016) 18-26.
- [6] S. Sharma, C. Periasamy, *Superlattices and Microstructures* 73 (2014) 12–21.
- [7] S. Khodja, T. Touam, A. Chelouche, F. Boudjouan, D. Djouadi, Z. Hadjoub, A. Fischer, A. Boudrioua, *Superlattices and Microstructures* 75 (2014) 485-495.
- [8] Á. Németh, Cs. Major, M. Fried, Z. Lábadi, I. Bársony, *Thin Solid Films* 516 (2008) 7016-7020.
- [9] C. Besleaga, G.E. Stan, A.C. Galca, L. Ion, S. Antohe, *Applied Surface Science* 258 (2012) 8819-8824.
- [10] S. Logothetidis, A. Laskarakis, S. Kassavetis, S. Lousinian, C. Gravalidis, G. Kiriakidis, *Thin Solid Films* 516 (2008) 1345-1349.
- [11] D. Pal, J. Singhal, A. Mathur, A. Singh, Su. Dutta, S. Zollner, S. Chattopadhyay, *Applied surface science* (2016).
- [12] Z. Montiel-González, O. A. Castelo-González, M. T. Aguilar-Gama, E. Ramírez-Morales, H. Hu, *Appl. Therm. Eng.* (2016).
- [13] M. Gilliot, A. Hadjadj, A. En Naciri, *APPLIED OPTICS* 54 (2015) 3043-3050.
- [14] N. Ehrmann, R. Reineke-Koch, *Thin Solid Films* 519 (2010) 1475-1485.
- [15] G.E. Jellison, F.A. Modine, *Appl. Phys. Lett.* 69 (3) (1996) 371-373.
- [16] L. Miao, S. Tanemura, L. Zhao, X. Xiao, X. T. Zhang, *Thin Solid Films* 543 (2013) 125-129.
- [17] J.M. Khoshman, J.N. Hilfiker, N. Tabet, M.E. Kordesch, *Applied Surface Science* 307 (2014) 558-565.
- [18] H. A. Al-Khanbashi, W. Shirbeeny, A.A. Al-Ghamdi, L. M. Bronstein, W. E. Mahmoud, *Spectrochimica Acta Part A: Molecular and Biomolecular Spectroscopy* 118 (2014) 800-805.
- [19] M. Gilliot, C. Eypert, A. Hadjadj, *J. Appl. Phys.* 114 (2013) 183513.

- [20] Y.-S. Kim, W.-P. Tai, S.-J. Shu, *Thin Solid Films* 491 (2005) 153-160.
- [21] R.M.A. Azzam, N.M. Bashara, *Ellipsometry and Polarized Light*, North-Holland, Amsterdam, 1977.
- [22] H.-Q. Huang, F.-J. Liu, J. Sun, J.-W. Zhao, Z.-F. Hu, Z.-J. Li and X.-Q. Zhang, *Journal of Physics and Chemistry of Solids* 72 (2011) 1393-1396.
- [23] C.-H. Shih, I. Lo, W.-Y. Pang and C.-H. Hsieh, *Journal of Physics and Chemistry of Solids* 71 (2010) 1664-1668.
- [24] X.Q. Wei, Z.G. Zhang, M. Liu, C.S. Chen, G. Sun, C.S. Xue, H.Z. Zhuang, B.Y. Man, *Mater. Chem. Phys.* 101 (2007) 285-290.
- [25] J. Ye, S. Gu, S. Zhu, T. Chen, L. Hu, F. Qin, R. Zhang, Y. Shi, Y. Zheng, *J. Cryst. Growth* 243 (2002) 151-156.
- [26] S. Singh, P. Chakrabarti, *Superlattices and Microstructures* 64 (2013) 283-293.
- [27] L. Znaidi, *Mater. Sci. Eng. B* 174 (2010) 18-30.
- [28] P. Hoyer, H. Weller, *Chem. Phys. Lett.* 221 (1994) 379-384.
- [29] A.-S. Keita, A. En Naciri, F. Delachat, M. Carrada, G. Ferblantier, A. Slaoui, *J. Appl. Phys.* 107 (2010) 093516.
- [30] M.-B. Bouzourâa, A. En Naciri, A. Moadhen, H. Rinnert, M. Guendouz, Y. Battie, A. Chaillou, M.-A. Zaïbi, M. Oueslati, *Materials Chemistry and Physics* 175 (2016) 233-240.
- [31] H. Fujiwara, *Spectroscopic Ellipsometry: Principles and Applications*, Wiley, Japan, 2007.
- [32] E.D. Palik, *Handbook of Optical Constants of Solids*, Elsevier, London, 1997.
- [33] A. En Naciri, P. Miska, A.-S. Keita, Y. Battie, H. Rinnert, M. Vergnat, *J. Nanopart. Res.* 15 (2013) 1538.
- [34] R.J. Gehr, R.W. Boyd, *Chem. Mater* 8 (1996) 1807-1819.
- [35] M. Dressel, G. Grüner, *Electrodynamics of Solids, Optical Properties of Electrons in Materials*, Cambridge University, Press Cambridge, 2002.
- [36] A.R. Forouhi, I. Bloomer, *Phys. Rev. B* 34 (1986) 7018-7026.
- [37] C. Tanguy, *Phys. Rev. Lett.* 75 (1995) 4090-4093.
- [38] G. E. Jellison, A. Boatner, *Phys. Rev. B* 58, (1998) 3586-3589.
- [39] K. Postava, H. Sueki, M. Aoyama, T. Yamaguchi, C. Ino, Y. Igasaki, M. Horie, *J. Appl. Phys.* 87, (2000) 7820-7824.
- [40] R. Hauschild, H. Priller, M. Decker, J. Brückner, H. Kalt, C. Klingshirn, *Phys. Stat. Sol.* 4, (2006) 976-979.
- [41] P. L. Washington, H. C. Ong, J. Y. Dai, R. P. H. Chang, *Appl. Phys. Lett.* 72 (1998) 3261-3263.

- [42] A. Djuricic, Y. Chan, E. Li, *Applied Physics A* 76 (2003) 37–43.
- [43] F. Jiang, J. Dai, L. Wanga, W. Fanga, Y. Pua, Q. Wang, Z. Tang, *Journal of Luminescence* 122–123 (2007) 162-164.
- [44] G. Nam, H. Park, H. Yoon, J. S. Kim, J.-Y. Leem, *Current Applied Physics* 13 (2013) S168-S171.
- [45] C. Klingshirn, *Phys. Status Solidi B* 71 (1975) 547-556.
- [46] W.Y. Liang, A.D. Yoffe, *Phys. Rev. Lett.* 20 (1968) 59-62.
- [47] Y. Toyozawa, J. Hermanson, *Phys. Rev. Lett.* 21 (1968) 1637-1641.
- [48] M. S. Ramachandra Rao, T. Okada, *ZnO Nanocrystals and Allied Materials*, Springer, India, 2014.
- [49] L. J. Wang, N. C. Giles, *J. Appl. Phys.* 94 (2003) 973-978.
- [50] Y.P. Varshni, *Physica* 34 (1967) 149-154.
- [51] G.D. Cody, *Hydrogenated Amorphous Silicon, Semiconductors and Semimetals Part b*, Pankove, New York, 1984.
- [52] B. K. Meyer, H. Alves, D. M. Hofmann, W. Kriegseis, D. Forster, F. Bertram, J. Christen, A. Hoffmann, M. Straßburg, M. Dworzak, U. Haboeck, A. V. Rodina, *phys. stat. sol. (b)* 241 (2004) 231-260.
- [53] D. G. Thomas, *J. Phys. Chem. Solids* (1960) 86-96.
- [54] R. Hauschild, H. Priller, M. Decker, J. Brückner, H. Kalt, C. Klingshirn, *phys. stat. sol. (c)* 3 (2006) 976-979.